YMTHE, Volume *31*

Supplemental Information

Structural and functional characterization of capsid binding by anti-AAV9 monoclonal antibodies from infants after SMA gene therapy

Grant J. Logan, Mario Mietzsch, Neeta Khandekar, Arlene D'Silva, Daniel Anderson, Mawj Mandwie, Jane Hsi, Austin R. Nelson, Paul Chipman, Jennifer Jackson, Peter Schofield, Daniel Christ, Christopher C. Goodnow, Joanne H. Reed, Michelle A. Farrar, Robert McKenna, and Ian E. Alexander

Table S1. V, D, and J gene usage in reconstituted anti-AAV9 mAb (Excel file).

Table S2. Concentration of mAb to produce 50% of maximal absorbance by anti-AAV9 IgG ELISA

EC50 (ng/mL)	Pt1	Pt2	Pt3
mAb1	5.0	7.7	4.9
mAb2	5.3	11.7	5.0
mAb3	6.5	13.3	5.0
mAb4	15.1	7.1	138.2
mAb5	9.7	5.2	17.1
mAb6	6.7	5.3	4.8
mAb7	113.6	8.5	29.6

Table S3. Concentration of mAb to inhibit 50% of AAV9 vector functional transduction

IC50 (ng/mL)	Pt1	Pt2	Pt3
mAb1	4.4	8.1	2.2
mAb2	2.4	11.7	1.8
mAb3	4.7	5.5	4.6
mAb4	4.0	6.2	*
mAb5	2.6	3.0	8.8
mAb6	2.3	4.9	2.8
mAb7	104.9	24.4	6.1

* mAb did not completely neutralize in the antibody dilution range and an IC50 value could not be calculated

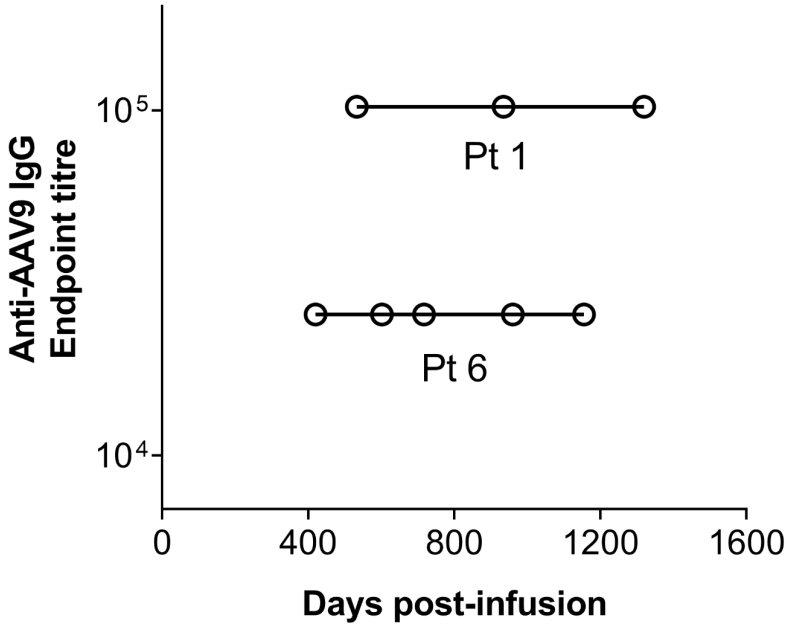

Figure S1. Anti-AAV9 IgG responses are durable and sustained beyond 42 months post-treatment. Anti-AAV9 IgG endpoint titers in two treated infants were measured by ELISA. The x-axis indicates day of serum collection post-AAV infusion.

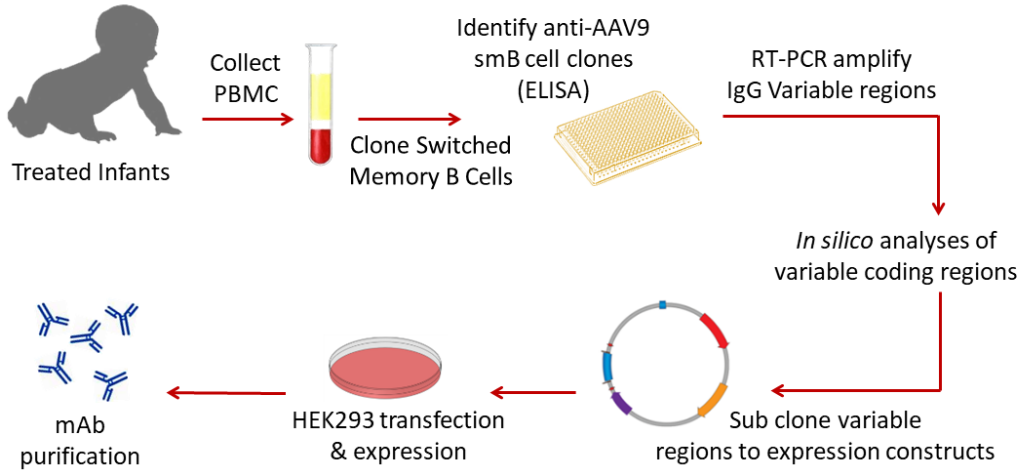

Figure S2. Strategy overview to clone and reconstitute mAb from treated infants.

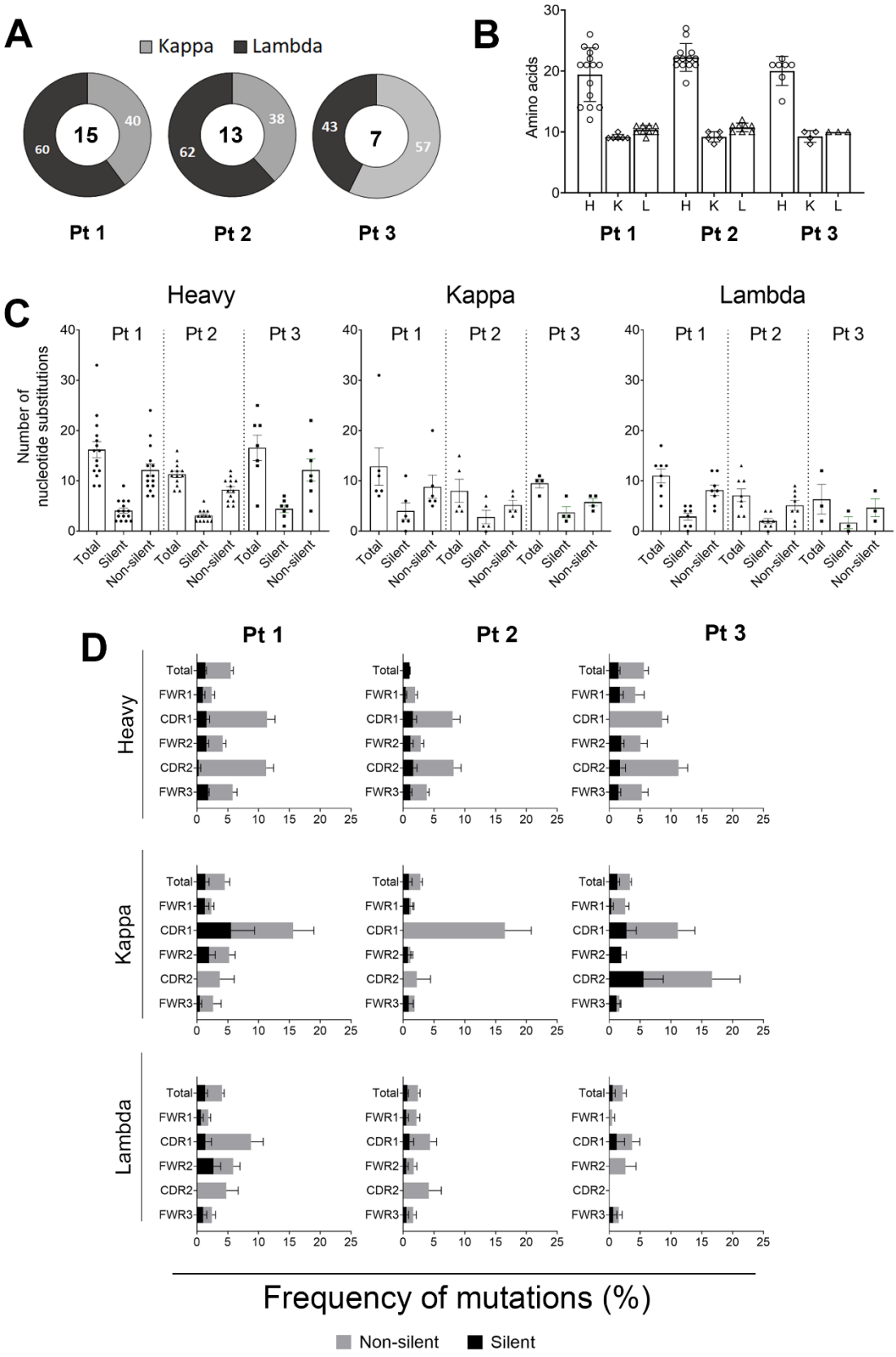
A
Kappa
Lambda
15
40
60
13
38
62
7
43
57
Pt 1
Pt 2
Pt 3
B
Amino acids
H K L H K L H K L
Pt 1
Pt 2
Pt 3
C
Heavy
Kappa
Lambda
Number of nucleotide substitutions
Total
Silent
Non-silent
D
Heavy
Kappa
Lambda
Total
FWR1
CDR1
FWR2
CDR2
FWR3
Frequency of mutations (%)
Non-silent
Silent

Figure S3. *In silico* characterization of nucleotide and amino acid sequences of light and heavy chain antibody variable regions encoded by anti-AAV9 reactive smB cell clones. (A) Kappa or lambda antibody light chain usage in of 35 mAb isolated from the three treated infants. The numeral in the center of each graph is the total number of reconstituted anti-AAV9 reactive mAbs for each infant. (B) Amino acid length of CDR3 for each light and heavy chain antibody sequence (H, heavy; K, kappa; L, lambda) (C) Frequency of synonymous and non-synonymous nucleotide changes in light and heavy chain antibody sequences. (D) Frequency of synonymous and non-synonymous changes with respect to framework (FW) regions, CDR1 and CDR2. Dots in (B) and (C) indicate values for individual antibody chains. Bars in (B), (C) and (D) indicate the mean for each group. Error bars indicate the standard error of the mean.

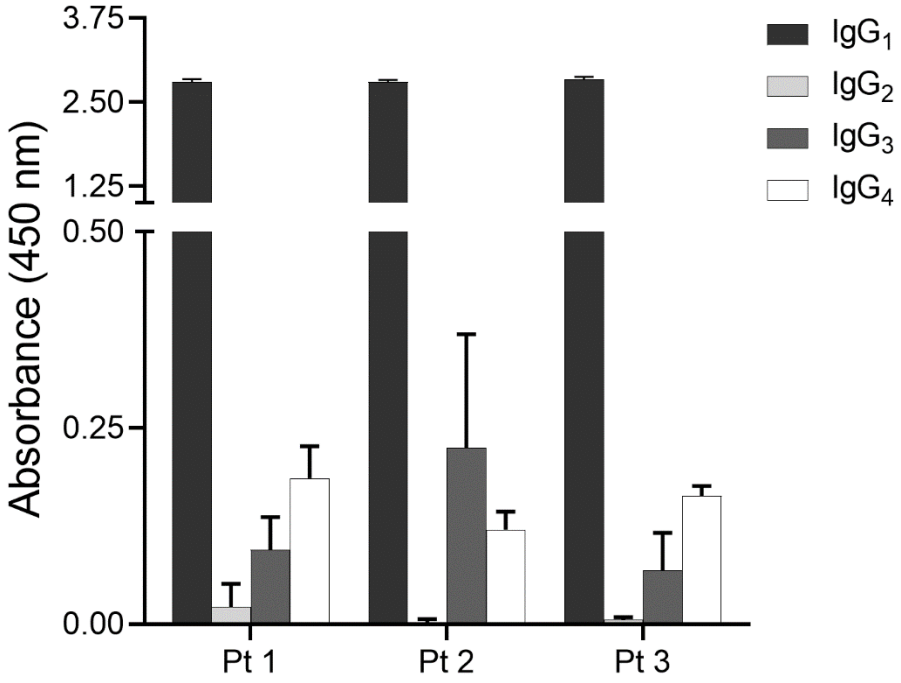

Figure S4. Prevalence of IgG subclass reactive to AAV9 in patient sera. ELISA for anti-AAV9 IgG was performed on sera (diluted 1:100) from Pts 1-3 and analyzed to determine the prevalence of IgG subclasses 1-4. Bars indicate the mean absorbance and error bars indicate standard deviation from the data pooled from three independent ELISA.

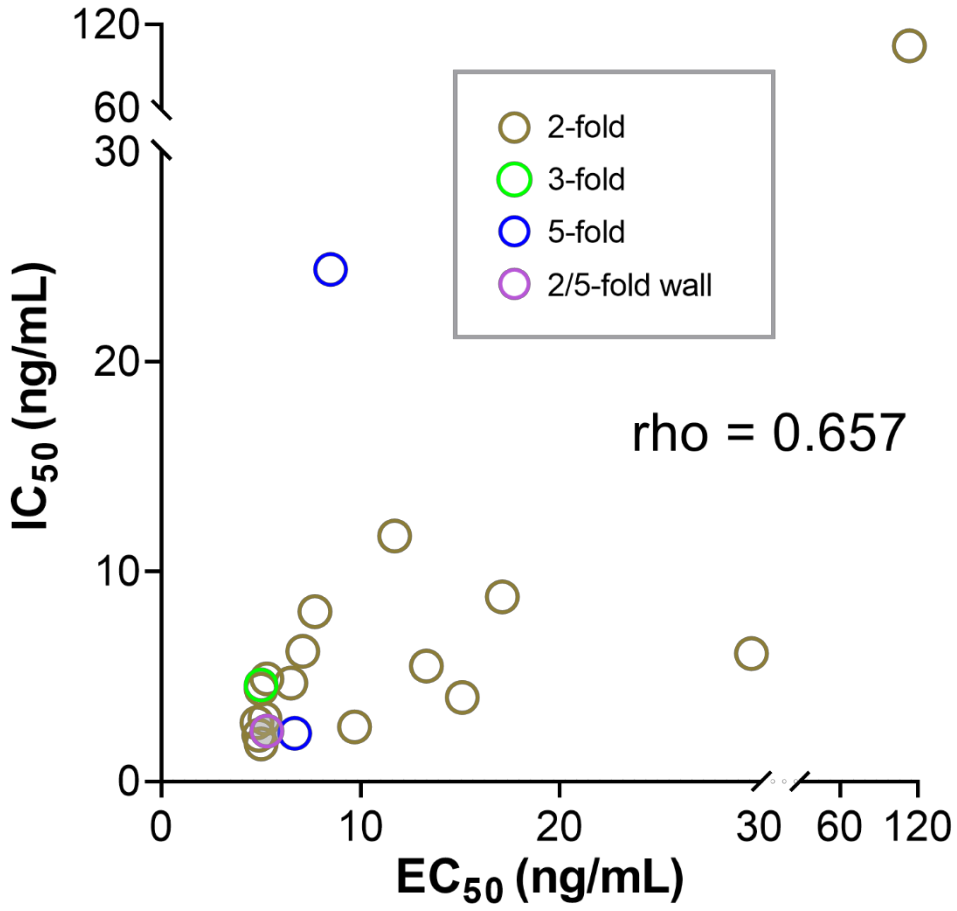

Figure S5. Correlation between EC_{50} and IC_{50} values. Each circle represents an individual mAb that has been color-coded to indicate capsid binding location. mAb 3-4 is not shown as it did not produce an IC_{50} value across the mAb concentrations tested. The Spearman rho test shows a modest correlation (rho = 0.657 with 95% confidence interval 0.289 – 0.856, Graphpad Prism).

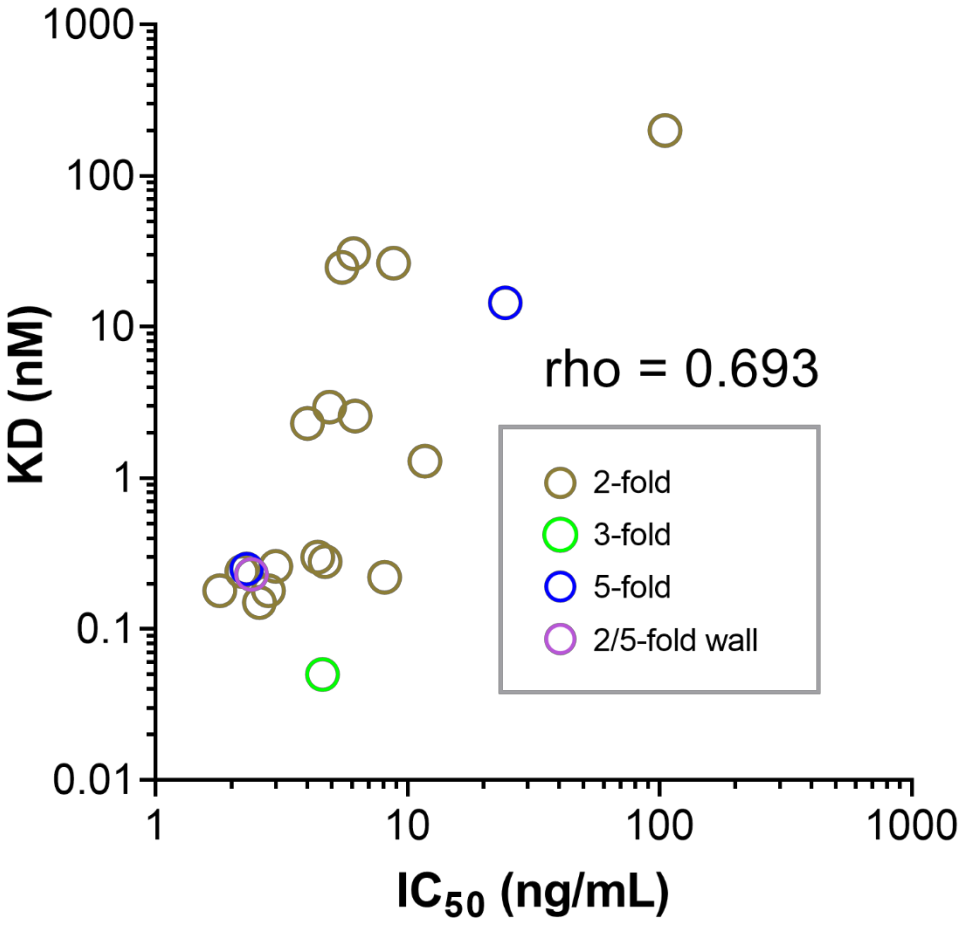

Figure S6. Correlation between mAb IC_{50} and Fab binding affinity. Each circle represents an individual mAb that has been color-coded to indicate capsid binding location. mAb 3-4 is not shown as it did not produce an IC_{50} value across the mAb concentrations tested. The Spearman rho test shows a modest correlation (rho = 0.693 with 95% confidence interval 0.349 – 0.872, Graphpad Prism).